Analysis & Sensing

Chemistry Europe
European Chemical Societies Publishing

Accepted Article

Title: Real-Time Non-Faradaic Potentiodynamic Impedance Sensing Using Screen-Printed Carbon Electrodes

Authors: Emil Fuhry, Victoria Guglielmotti, Isabell Wachta, Diego Pallarola, and Kannan Balasubramanian

To be cited as: *Anal. Sens.* **2024**, e202400037

Link to VoR: https://doi.org/10.1002/anse.202400037

WILEY VCH

Real-Time Non-Faradaic Potentiodynamic Impedance Sensing Using Screen-Printed Carbon Electrodes

Emil Fuhry[1], Victoria Guglielmotti[1,2], Isabell Wachta[1], Diego Pallarola[2*], Kannan Balasubramanian[1*]

[1]Department of Chemistry, School of Analytical Sciences Adlershof (SALSA) & IRIS Adlershof, Humboldt-Universität zu Berlin, Berlin, Germany.

[2]Instituto de Nanosistemas, Universidad Nacional de General San Martín, San Martín, 1650 Provincia de Buenos Aires, Argentina

**Corresponding author e-mail:* dpallarola@unsam.edu.ar , nano.anchem@hu-berlin.de

ABSTRACT

Electrochemical impedance spectroscopy (EIS) is a suitable analytical technique to detect interfacial phenomena and analyte binding at electrode surfaces. In contrast to metallic electrodes, carbon-based electrodes are more suited due to the low cost and the availability of more versatile methods for chemical functionalization. For (bio) sensing, often the Faradaic version of EIS in a three-electrode configuration is used, where a redox-active species is used as a marker. In order to avoid interference due to the redox-active marker with the interfacial interaction, we focus here on the use of non-Faradaic EIS in the absence of any added markers. First, we utilize the sedimentation of silica beads as a model system, which reduces the complexity of the interaction simplifying the interpretation of the measured signals. Moreover, we introduce two improvements. First, impedance measurements are performed in a three-electrode configuration with applied potential as an additional variable, which serves as a handle to optimize the sensitivity. Secondly, we present a time-differential strategy to detect subtle changes and demonstrate that we can consistently follow the sedimentation of beads using the non-Faradaic impedance as a function of the applied potential. Finally, we show a

proof-of-principle demonstration for the biosensing of cell attachment on the electrodes in real-time using the proposed technique.

Keywords. point of zero charge, capacitive sensors, electrochemical impedance spectroscopy (EIS), cell sensing, electric cell-substrate impedance sensing (ECIS), potentiodynamic, screen-printed electrodes, adsorption

Introduction

Electrochemical Impedance Spectroscopy (EIS) is a highly promising transduction strategy for biosensing. [1] It is widely used for the detection of analyte binding or for monitoring interfacial interactions. [2] In Faradaic EIS, a redox-active species is used as a marker to detect the occurrence of the interfacial event. [3] Ideally, an equivalent circuit is derived from the experimental data. The charge transfer resistance, which characterizes the electron transfer (ET) with the added redox-active marker, increases in the presence of interfacial adsorption. By following this in real-time, it is possible to decipher the kinetics of interfacial interactions. [4] Indeed, it has been shown that the adsorption of single particles can be followed by strategies that exploit changes in charge transfer. [5]

There are however some drawbacks in this sensing methodology. [6] First, the presence of a marker only for detection purposes may affect the interfacial interaction itself. This could be due to the oxidizing or reducing ability of the added redox species. But there may also be other kinds of interactions either with the receptor immobilized on the electrode surface, or with the analyte molecules in solution, e.g. denaturation. [7] Second, the impedance measurements are typically carried out at the open circuit potential (OCP), [8] which is expected to correspond to the formal potential of the added redox-active species. This assumption is however only valid when the effective OCP at the electrode is exclusively determined by the added redox-active species. Often, there may be other redox-active species (either intentionally added or not) in the

medium, which will effectively contribute to a mixed potential at the electrode surface. [9] As a result, ET with the different redox-active species and its blocking may vary during the sensor trial, which makes the interpretation of the sensor signals very difficult. In some cases, a constant potential corresponding to the formal potential of the redox species is enforced during the acquisition of the impedance spectra. [5a]

An alternative strategy to overcome these drawbacks is the use of non-Faradaic impedance spectra, which are acquired in the absence of added redox-active markers. [6a, 10] This transduction strategy has been successfully deployed to detect DNA, proteins and cells. [2b, 11] Often a two-electrode configuration is utilized, where both electrodes are made of the same material. Commonly, the impedance at a selected frequency is measured between the two electrodes and the imaginary part of the impedance (often just referred to as capacitance) serves as the sensor signal. Since non-Faradaic impedance aims mainly at the interrogation of the electrical double layer (EDL), it is necessary to realize specialized electrodes placed close to each other (e.g. by microstructuring). [10-12] Using the two-electrode configuration, particle size of the beads in the vicinity could be estimated using non-Faradaic impedance. [13] Sedimentation of beads was however not discussed here.

Here, we utilize the standard three-electrode electrochemical cell in the form of a carbon screen printed electrode (SPE) to investigate the use of non-Faradaic EIS for sensing. Carbon, as a working electrode, has the advantage that it is insensitive to chloride in solution, which is in contrast to gold. [1b, 14] Moreover, carbon offers a broader electrochemical window free of catalytic effects. [15] Furthermore, temporal drifts in impedance response are expected to be intrinsically relatively lower with carbon as a working electrode. [16] Typically, in three-electrode measurements, the electrochemical (direct current – DC) potential is kept constant [6b] if not left to float at OCP. The effect of a variation in this potential has seldom been systematically studied in a sensing context.[17]

In this work, we investigate the effect of the applied DC potential on the non-Faradaic impedance response. As a model system, we chose to use the sedimentation of beads on the electrode. [5, 18] This system is ideally suited because the beads settle down quite rapidly on the electrode surface. [19] Moreover, since the interaction is non-specific, we avoid complications due to variation in capture probe density (as dictated by functionalization efficiency) [20] or the kinetics of adsorption, [5a] which may render the interpretation of the impedance response difficult. It provides us with a clean model system, where we can clearly distinguish between two states – bound versus non-bound. [5b] This enables us to extract the impedance spectra for each of the two cases and achieve an unambiguous interpretation of the measured data. Moreover, they are totally redox inactive and hence are well-suited for understanding non-Faradaic EIS. Using beads also enables easy surface regeneration, [21] which is absolutely necessary to use the same sensor chip for testing reproducibility. Based on the understanding gained from these experiments, we demonstrate that the technique can be exploited to monitor the real-time attachment of cells [22] on to the electrode without the need for labeling.

Usually, one of the reasons for measuring at open circuit is the need to avoid polarization impedance in EIS. [23] Under applied potential, with added redox-active markers, the kinetics of charge transfer and diffusion effects will lead to variations in the measured impedance spectra over time. In the absence of redox-active markers, however, we can identify a potential range, where Faradaic reactions are mostly avoided. We find here that, by choosing an optimal potential, the sensitivity to bead adsorption on the sensor surface can be maximized. This avoids the need for any kind of microstructuring, which has often been used to improve sensitivity. [24] Moreover, residual variations in the impedance response due to polarization, diffusion or kinetic effects can be further minimized by employing a time-differential strategy. Here, the potential-dependent impedance after analyte addition is measured relative to the situation in the absence of analyte. Thus, we can cancel out the effect of any residual temporal impedance variations

enabling us to extract the potential dependent impedance response, almost exclusively due to analyte adsorption on the electrode.

Results and Discussion

Figures 1(a) and 1(b) present a scheme of our measurement and a photo of the sensor chip. We use commercial screen-printed electrodes with carbon as working and counter electrodes and Ag/AgCl paste as the reference electrode (see electron microscopy images in figure S1 in supporting information (SI)). The sensor response is measured in a microwell (volume: 150 µL) placed above the sensor chip. The impedance spectrum is continuously acquired as the potential is (cyclically) swept between two chosen vertex potentials. The impedance is acquired in a frequency range of 5 Hz – 100 kHz and the potential stepped at 30 mV. The measurements start in blank electrolyte, followed by addition of the bead solution (silica beads, 7 µm diameter, 5 w/v %) at a chosen time instant.

Figure 2(a) presents the cyclic voltammogram measured at a typical carbon SPE in 0.1 M KCl without any added redox-active species. It is apparent that the response is purely capacitive in the middle of the measured potential range. At the extreme potentials, we see a current onset mostly due to redox reactions such as oxygen reduction and water oxidation. In order to extract information from the impedance spectrum, it is necessary to model it using an equivalent circuit. Figure 2(b) presents the impedance spectrum obtained at an applied potential of 0 V vs. Ag/AgCl, together with fits based on two different equivalent circuits (see figure 1(c)). In the first case, we model the interface using a simple R_s - Q circuit, which is common in non-Faradaic EIS. [2b, 21, 25]. Here Q is a capacitive constant phase element, [2b, 26] whose impedance Z_Q is given by $Z_Q^{-1} = C_\alpha(\mathrm{j}\,\omega)^\alpha$ with C_α the non-ideal capacitance and α the order (which is a measure of the non-ideality of the capacitance) in the range $0 < \alpha \leq 1$, $j = \sqrt{-1}$, and ω is the angular frequency. R_s refers to all resistive components in series, including the electrode and

solution resistance. C_α is a measure of the interfacial capacitance, which includes the double layer capacitance, as well as the capacitance due to surface inhomogeneities. [2b]

It is apparent that at very low frequencies, the fit is not ideal (blue phase curve in figure 2(b)). It can be improved by using a second model (R_s - (Q || R_{CT})) (see figure 1(c)), which includes an additional resistance (R_{CT}) in parallel with the interfacial capacitance. Indeed, such a model is typically used in EIS, when a redox-active species is present in solution, and is referred to as simplified Randles circuit. [2b] Here R_{CT} is referred to as the charge transfer resistance, attributed to a Faradaic process. Although we do not have any added redox species, background Faradaic processes occurring in ambient, especially at extreme potentials, cannot be avoided, such as oxygen reduction and water oxidation. The value of the resistance in this fit is relatively high (around 1.1 MΩ, see fitting details in table T1 in SI). Hence the appearance of R_{CT} can indeed be attributed to trace amounts of residual redox-active species dissolved in ambient (e.g. O_2), which may contribute to the effective impedance.

Utilizing the impedance spectra measured at various applied potentials, we perform a model fit at every potential and extract the model parameters R_s, Q and R_{CT}. Figure 2(c) presents the dependence of C_α as a function of potential in blank electrolyte, while figure 2(d) shows the relative error in the fit using the two models. The curve in figure 2(c) shows that the capacitance varies as a function of applied potential, which is expected. [23, 27] The capacitance at the electrode-electrolyte interface comprises of two components – a diffuse layer and a double layer capacitance. The variation of the potential leads to a reorganization of the double layer structure resulting in a modulation of the net capacitance. The potential of lowest capacitance is referred to as the potential of zero charge (pzc). [27b] The peculiar shape of the potential-dependent C_α profile can be attributed to the heterogeneity of the carbon surface, similar to observations on polycrystalline metal electrodes. [27] The same pzc and the potential dependent profile was seen in all the carbon SPEs we measured, although the magnitude of C_α varied up to one order of magnitude from one device to the other.

Using the more elaborate (R_s - (Q || R_{CT})) model, the fit error in C_α is reduced at most by half (orange curve in figure 2(d)). The improvement is prominent at the potential extremes. Consistent with the previous discussion, this can be attributed to background redox reactions in the buffer (e.g. due to oxygen reduction and water oxidation), which start playing an active role at extreme potentials. Hence the second model including R_{CT} (corresponding to these reactions) fits the data better in this potential region, although the improvement is rather minimal. Using either of the two models, there is no substantial difference between the two potential-dependent profiles of the interfacial capacitance (figure 2(c)). The potential dependence of the other parameters is discussed in figure S2 in SI. In order to improve the measurement speed, we chose to measure the impedance at two frequencies per decade. With this lower frequency resolution, the data can be fit better with the two-parameter R_s-Q model. Hence, we will use the simpler R_s-Q model for the rest of the discussion.

First, we present the effect of bead adsorption on the potential-dependent C_α profile. For this purpose, we measure the impedance response in blank electrolyte and subsequently add a solution (with the same electrolyte) containing silica beads/particles (5 w/v%) to the microwell. By optical microscopy (see figure S3 in SI) we observe that the added beads rapidly sediment on the sensor surface. After a few minutes, the impedance spectrum is acquired with the adsorbed beads. Figure 3(a) presents the potential-dependent C_α profile obtained without and with silica beads adsorbed on the sensor surface. It is apparent that the profile has changed due to the presence of the adsorbed bead layer. This can be attributed to a change in the interfacial structure, whereby the beads cause a change in the interfacial charge density as well as a modification of the pzc. While a change in pzc is known to shift the potential-dependent capacitance along the potential axis, a change in interfacial charge density causes a modification of the capacitance profile. [27]

In order to clearly identify the change in capacitance due to the beads, we use the initial potentiodynamic C_α profile at the time of bead addition as a baseline (C_0) and correct the dataset

for adsorbed beads (C_t , the capacitance measured at time t) using this baseline. Figure 3(b) presents this baseline corrected or time-differential profile of the same data, where the change in capacitance is plotted as percentage change given by $\Delta C_\alpha = 100\ (C_t - C_0)/C_0$. This time-differential plot directly gives an idea, where the maximal change in capacitance is observed. For the present case of silica beads in 0.1 M KCl, we find that the maximum change (around 14%) is positive and occurs at around +0.15 V. In purely capacitive biosensors, capacitance (measured at a constant frequency) was found to decrease or increase depending on the application. [11, 28] This can be understood based on the data in figure 3(a). A change in the interfacial ionic structure due to analyte adsorption can be expected to cause a change in pzc and a modulation of the interfacial charge density. This will result in a modified potentiodynamic C_α curve. Hence, the change in capacitance will depend on the applied potential and can be zero, positive or negative. It is also important to note that, in contrast to previous works, our measurements are done in a three-electrode configuration and we extract the capacitance using an equivalent circuit fitted to the entire impedance spectrum.

Now we turn towards the actual methodology for recording the real-time sensor response during the sedimentation of beads. We continuously acquire potential dependent impedance spectra and extract C_α and R_s from every such spectrum. Figure 3(c) presents a map of the extracted capacitance C_α as a function of potential and time. The measurement is started in blank electrolyte and the beads are added at the time instant t = 0. Upon addition, a clear change in the potentiodynamic C_α is visible in the map. In order to visualize this change more clearly, figure 3(d) shows the time-differential map ΔC_α extracted from this data. As mentioned earlier, the change in capacitance is rapid after the addition of beads due to the sedimentation of the beads directly on to the electrode surface. After sedimentation, there is little change in the capacitance over the rest of the time period. These observations are consistent with previous EIS measurements of beads on sensor surfaces. [5b, 19].

We have also analyzed the potential dependence of sensitivity in the fitted parameter R_s. Figure 4(a) shows a time-differential map of the evolution of this parameter (ΔR_S) as a function of potential and time. Upon addition of beads, a change in the parameter is actually observed, which is also found to vary as a function of potential (see figure 4(b)). However, this change is very weak and at least an order of magnitude lower than that of ΔC_α. This observation further confirms that we are observing mainly a capacitive change at the electrode-electrolyte interface due to the adsorption of beads. We have achieved this here in a three-electrode configuration of the carbon SPE without any specialized electrode layout (microstructuring) or addition of redox-active species. A possible explanation for the mechanism of sensor response is discussed in SI (figure S7).

For the sake of comparison, we have also applied our measurement strategy for Faradaic EIS, where we study the sedimentation of beads on the same carbon SPE sensors, but now in the presence of an added redox marker in the solution. Here, we have used ferreocenedimethanol (FDM) at a concentration of 0.1 mM as the redox marker. For Faradaic EIS, R_{CT} is the key parameter. [2b] Figure 5(a) presents the evolution of the time-differential R_{CT} as a map, while figure 5(b) presents the potential-dependent sensitivity ΔR_{CT} overlaid over the CV. R_{CT} increases upon bead absorption, consistent with the blocking of charge transfer to FDM due to the presence of the adsorbed bead, similar to previous observations. [5] It is apparent that the maximum sensitivity is attained at a potential, which corresponds to the formal potential (as observed in the CV) of the added redox marker FDM. Moreover, the change in this parameter is much larger than what we observed for ΔC_α in the non-Faradaic case. This is consistent with expectations that Faradaic EIS is in general more sensitive than non-Faradaic EIS, provided the measurements are performed at a controlled potential. Moreover, by varying the concentration of FDM, the magnitude of R_{CT} can be varied, using which we can modulate the sensitivity to some extent. As mentioned earlier, all these advantages can be exploited only when the redox

species does not interfere with solution components or with the sensing interaction at the interface.

Finally, as a proof-of-principle, we demonstrate the application potential of our methodology by studying the non-specific adsorption of MCF-7 cancer cells on to the carbon SPE. Details of cell culture can be found in the experimental section. [29] Figures 6(a) and (b) present a map of time-differential potentiodynamic C_α and R_s extracted from impedance spectra measured continuously during the attachment of MCF-7 cells to the blank solution at t = 0. In both cases, we see a change after the addition of the cells. ΔC_α shows a variable change depending on the applied potential. Moreover, the change is dynamic over time. The cells are more dynamic than the beads and the attachment of cells on the carbon surface is expected to show some kinetics over time, since the adhesion to the electrode is progressive and relatively slower (see optical images figure S4 in SI). Moreover, changes in cell morphology may occur after cell attachment. [29] The differential resistance plot (figure 6(b)) shows a change as a function of potential, however, the change over time is rather constant. Moreover, its magnitude is rather low, in comparison to the large changes observed in the ΔC_α channel. This again attests the fact that we mainly observe capacitive changes due to cell attachment. In order to minimize damage to the cells, we restrict the potential range to $0 < E < 0.5$ V.

In order to understand the temporal evolution of the map, figure 6(c) compares the potentiodynamic C_α profile before and 10 minutes after attachment of the cells. It is clear that the presence of cells at the interface leads to a cathodic shift of the potential dependent C_α profile, indicating a change in pzc towards negative potentials. As a result, we see a negative change in capacitance for potentials $E < 0.3$ V and a positive change in capacitance for $E > 0.3$ V, as exemplified by the differential C_α plot in figure 6(d). Previous works on using EIS for cell adhesion have reported both increase and decrease in capacitance. [11, 28] Our results provide an explanation for these apparent contradictory observations. We showed here that the presence of a cell layer shifts the pzc along the potential scale. Hence, the potential at the electrode (either

applied or pre-determined by the solution constituents and measurement condition) will determine the polarity of the capacitance change. In this manner, our strategy not only provides a method to sensitively detect analyte adsorption on the electrode surface but also provides hints on changes in the pzc due to the presence of adsorbed analyte species.

Conclusion

In conclusion, we have demonstrated that potentiodynamic non-Faradaic EIS is a suitable strategy to study interfacial adsorption in screen-printed carbon sensors. We showed that the impedance response can be fitted with a simple R_s-Q model, which enables the extraction of the interfacial non-ideal capacitance unambiguously. By monitoring this interfacial capacitance as a function of applied potential in real-time, we demonstrated that the sensitivity to analyte adsorption is maximized at certain applied potentials. This could be corroborated with a change in the non-ideal-capacitance-voltage profile, which partly arises due to a change in pzc after analyte adsorption. We showed that our measurement strategy is also applicable for Faradaic EIS, where we can identify the optimal applied potential. Irrespective of the mode being Faradaic or not, using our time-differential potentiodynamic EIS sensing strategy, one can identify the potential at which maximal sensitivity towards analyte adsorption can be attained. This technique can now be extended to study biomolecule adsorption and determine the optimal conditions for maximizing the sensor response free of added redox-active markers.

Experimental Section

Chemicals. All chemicals were sourced from commercial suppliers, and used without further purification. 1,1'-ferrocenedimethanol (CAS: 1291-48-1) was purchased from Sigma-Aldrich, Germany; potassium chloride (KCl, CAS: 7447-40-7) from Merck KGaA Germany, glue (Hartkunstoff Spezialkleber) from UHU GmbH & Co. KG, Germany. Silica particles (6.98µm, SD=0.19µm, aqueous suspension) were purchased from microParticles GmbH. The carbon screen printed electrodes (11L) were purchased from DropSens Metrohm Germany. All solutions were prepared with ultra-pure water (Barnstead Easypure II system, 18.2 MΩ.cm^{-1}).
Surface characterization. The optical images were captured using a Nikon Eclipse Ti2 inverted microscope or a Leica DM4000B fluorescence microscope. The SEM images were acquired

using a JEOL JCM-6000 Neoscope ESEM-EDX instrument in high-vacuum mode. The electrodes were electrically connected to the microscope stage. No coating or other pretreatment of the surface was applied. The measurements were conducted using secondary electron imaging at an intensity of 15 keV.

Electrochemical measurements. All electrochemical measurements were conducted in ambient within a shielded custom-made Faraday cage in a standard three-electrode set-up using an EmStat 4S PalmSens potentiostat. The data acquisition and analysis were performed with PSTrace (Version: 5.9.4206) Palmsens. For EIS measurements, the carbon SPE was fitted with a 250µl microwell on top. The working electrode area is approximately 12.5 mm^2. The counter electrode consists of carbon and the reference electrode is composed of Ag/AgCl. Impedance spectra were recorded every 45 seconds over a frequency range of 5 Hz – 100 kHz, by applying a sinusoidal AC voltage of 10 mV amplitude. Following each measurement, the applied potential was systematically varied between -0.3 V and 0.5 V, with a step size of 30 mV.

Silica particles/beads. The silica beads were washed at least 4x with the blank electrolyte used in the electrochemical measurement. For this purpose, the beads were centrifuged at 12000 g (MiniSpin, Eppendorf SE) and the supernatant was exchanged with the blank electrolyte. The beads are diluted to a final weight percentage of 5%. Then, the beads are resuspended and 10 µL of the suspension is added to 150 µL of blank electrolyte.

Cell measurements. The human epithelial breast cancer cell line (MCF-7, DSMZ no. ACC 115) was obtained from DSMZ Germany. These cells were cultured in RPMI supplemented with 10% fetal bovine serum (FBS), 1% sodium pyruvate, 1% alpha medium (MEM, 100 units/mL penicillin-streptomycin, and 1% non-essential amino acids (NEAA) at 37°C with 5% CO_2. All cell culture chemicals were from Bio & Sell, Germany. For the adhesion experiments, adherent cells were detached from the culture surface using trypsin-EDTA 0.05% (Sigma-Aldrich, Invitrogen, Germany) for 5 minutes at 37°C. The cell media was exchanged to blank electrolyte (150 mM KCl). Subsequently, the cells were seeded onto the electrode. Prior to the addition of the beads or cells, the electrochemical impedance measurements were allowed to stabilize for at least 30 minutes.

Time differential impedance spectroscopy: The measurement logic was implemented in a custom script as part of PSTrace (Version: 5.9.4206). The data processing and fitting to a R_s - Q or R_s - (Q || R_{CT}) electrical equivalent circuit was performed by a custom-written python script, implemented using the impedance python module.[30] To calculate the relative impedance changes, the baseline data was extracted from the blank measurements across all measured potentials. The baseline is determined by performing a linear fit on the data to model the drift prior to the addition of the beads. Subsequently the blank data is subtracted from the impedance data at each potential.

Optical images: The microscopic images of the MCF-7 cells and silica beads were captured in a custom-made optical cell. This optical cell consists of a 250 µL microwell attached to a glass slide. The experiments start by adding the beads/cells to 150 µL of blank electrolyte within the microwell. Subsequently, images were recorded at 10 second intervals. The optical measurements were conducted concurrently with the electrochemical measurement.

Acknowledgements

We acknowledge Prof. Rüdiger Tiemann for support in setting up the live-cell-imaging microscope.

Funding

This project was funded by a joint initiative of the Deutsche Forschungsgemeinschaft (DFG, German Research Foundation) (project: 431849238) and CONICET (project: 23120180100103CO). Partial funding from the DFG as part of the excellence initiative *via* the Graduate School of Analytical Sciences Adlershof (GSC1013 SALSA) is acknowledged. This

work has received funding from the European Union's Horizon 2020 research and innovation programme under the Marie Skłodowska-Curie grant agreement No. 872869. D.P. acknowledges financial support from the National Agency for the Promotion of Science and Technology (ANPCyT, PICT-2019-00905). V.G. acknowledges CONICET for a doctoral scholarship. D.P. is a staff researcher of CONICET.

Data Availability

The data that support the findings of this study are available from the corresponding author upon reasonable request.

References

[1] a) P. Kanyong, A. V. Patil, J. J. Davis, *Annu. Rev. Anal. Chem.* **2020**, *13*, 183-200; b) V. Pinkova Gajdosova, L. Lorencova, A. Blsakova, P. Kasak, T. Bertok, J. Tkac, *Current Opinion in Electrochemistry* **2021**, *28*, 100717.

[2] a) C. M. A. Brett, *Molecules* **2022**, *27*; b) E. Katz, I. Willner, *Electroanal.* **2003**, *15*, 913-947; c) T. Bertok, L. Lorencova, E. Chocholova, E. Jane, A. Vikartovska, P. Kasak, J. Tkac, *ChemElectroChem* **2019**, *6*, 989-1003.

[3] a) A. Bonanni, M. J. Esplandiu, M. I. Pividori, S. Alegret, M. del Valle, *Anal. Bioanal. Chem.* **2006**, *385*, 1195-1201; b) M. E. Strong, J. R. Richards, M. Torres, C. M. Beck, J. T. La Belle, *Biosens. Bioelectron.* **2021**, *177*, 112949.

[4] P. Lasserre, B. Balansethupathy, V. J. Vezza, A. Butterworth, A. Macdonald, E. O. Blair, L. McAteer, S. Hannah, A. C. Ward, P. A. Hoskisson, A. Longmuir, S. Setford, E. C. W. Farmer, M. E. Murphy, H. Flynn, D. K. Corrigan, *Anal. Chem.* **2022**, *94*, 2126-2133.

[5] a) B. Roehrich, E. Z. Liu, R. Silverstein, L. Sepunaru, *J. Phys. Chem. Lett* **2021**, *12*, 9748-9753; b) B. M. Quinn, P. G. van't Hof, S. G. Lemay, *J. Am. Chem. Soc.* **2004**, *126*, 8360-8361.

[6] a) S. Upasham, I. K. Banga, B. Jagannath, A. Paul, K.-C. Lin, S. Muthukumar, S. Prasad, *Biosens. Bioelectron.* **2021**, *177*, 112940; b) X. Luo, M. Xu, C. Freeman, T. James, J. J. Davis, *Anal. Chem.* **2013**, *85*, 4129-4134.

[7] H. T. N. Le, D. Kim, L. M. T. Phan, S. Cho, *Talanta* **2022**, *237*, 122907.

[8] T. Yoetz-Kopelman, Y. Ram, A. Freeman, Y. Shacham-Diamand, *Electrochim. Acta* **2015**, *173*, 630-635.

[9] a) C. Wagner, W. Traud, *Zeitschrift für Elektrochemie und angewandte physikalische Chemie* **1938**, *44*, 391-402; b) J. F. Baez, M. Compton, S. Chahrati, R. Cánovas, P. Blondeau, F. J. Andrade, *Anal. Chim. Acta* **2020**, *1097*, 204-213; c) J. Janata, *ECS Solid State Letters* **2012**, *1*, M29.

[10] D. Berdat, A. C. Martin Rodríguez, F. Herrera, M. A. M. Gijs, *Lab Chip* **2008**, *8*, 302-308.

[11] S. Weaver, M. H. Mohammadi, N. Nakatsuka, *Biosens. Bioelectron.* **2023**, *224*, 115014.

[12] L. Huang, C. Zhang, R. Ye, B. Yan, X. Zhou, W. Xu, J. Guo, *Talanta* **2024**, *266*, 124951.

[13] D. S. d. Bruijn, K. F. A. Jorissen, W. Olthuis, A. v. d. Berg, in *2021 21st International Conference on Solid-State Sensors, Actuators and Microsystems (Transducers)*, **2021**, pp. 1036-1039.

[14] X. Xu, A. Makaraviciute, J. Pettersson, S.-L. Zhang, L. Nyholm, Z. Zhang, *Sens. Actuat. B* **2019**, *283*, 146-153.

[15] R. M. Iost, F. N. Crespilho, L. Zuccaro, H. K. Yu, A. M. Wodtke, K. Kern, K. Balasubramanian, *ChemElectroChem* **2014**, *1*, 2070-2074.

[16] a) E. Ziino, S. Marnoto, J. M. Halpern, *ECS Trans.* **2020**, *97*, 737; b) P. Kanyong, J. J. Davis, *J. Electroanal. Chem.* **2020**, *856*, 113675.
[17] G. A. Ragoisha, A. S. Bondarenko, *Electrochim. Acta* **2005**, *50*, 1553-1563.
[18] A. Sapper, B. Reiss, A. Janshoff, J. Wegener, *Langmuir* **2006**, *22*, 676-680.
[19] C. Laborde, F. Pittino, H. A. Verhoeven, S. G. Lemay, L. Selmi, M. A. Jongsma, F. P. Widdershoven, *Nat. Nanotechnol.* **2015**, *10*, 791-795.
[20] M. S. Wiederoder, I. Misri, D. L. DeVoe, *Sens. Actuat. B* **2016**, *234*, 493-497.
[21] C. Berggren, P. Stålhandske, J. Brundell, G. Johansson, *Electroanal.* **1999**, *11*, 156-160.
[22] Y. Xu, X. Xie, Y. Duan, L. Wang, Z. Cheng, J. Cheng, *Biosens. Bioelectron.* **2016**, *77*, 824-836.
[23] P. B. Ishai, M. S. Talary, A. Caduff, E. Levy, Y. Feldman, *Meas. Sci. Technol.* **2013**, *24*, 102001.
[24] a) F. Asphahani, M. Thein, O. Veiseh, D. Edmondson, R. Kosai, M. Veiseh, J. Xu, M. Zhang, *Biosens. Bioelectron.* **2008**, *23*, 1307-1313; b) S. Arman, V. R. Gonçales, Y. Yang, R. D. Tilley, K. Gaus, J. J. Gooding, *Electroanal.* **2023**, *35*, e202300124.
[25] C. Berggren, B. Bjarnason, G. Johansson, *Instrum. Sci. Technol.* **1999**, *27*, 131-139.
[26] S. Holm, T. Holm, O. G. Martinsen, *PLoS One* **2021**, *16*, e0248786.
[27] a) G. Valette, A. Hamelin, *J. Electroanal. Chem. Interf. Electrochem.* **1973**, *45*, 301-319; b) A. N. Frumkin, O. A. Petrii, B. B. Damaskin, in *Comprehensive Treatise of Electrochemistry: The Double Layer* (Eds.: J. O. M. Bockris, B. E. Conway, E. Yeager), Springer US, Boston, MA, **1980**, pp. 221-289.
[28] a) N. Jo, B. Kim, S.-M. Lee, J. Oh, I. H. Park, K. Jin Lim, J.-S. Shin, K.-H. Yoo, *Biosens. Bioelectron.* **2018**, *102*, 164-170; b) K.-S. Lee, S.-M. Lee, J. Oh, I. H. Park, J. H. Song, M. Han, D. Yong, K. J. Lim, J.-S. Shin, K.-H. Yoo, *Sci. Rep.* **2020**, *10*, 13709.
[29] V. Guglielmotti, E. Fuhry, T. J. Neubert, M. Kuhl, D. Pallarola, K. Balasubramanian, *ACS Sensors* **2024**, *9*, 101-109.
[30] M. D. Murbach, B. Gerwe, N. Dawson-Elli, L.-k. Tsui, *The Journal of Open Source Software* **2020**, *5*, 2349:2341-2345.

10.1002/anse.202400037

FIGURES

Figure 1. (a) Scheme showing a schematic of the electrochemical detection scheme. (b) Photo of the sensor chip (Carbon SPE) with a microwell placed on top of the chip. Scale bar 1 mm. (c) Equivalent circuit models used for fitting the EIS response. R_S: series resistance, Q: constant phase element, R_{CT}: charge transfer resistance

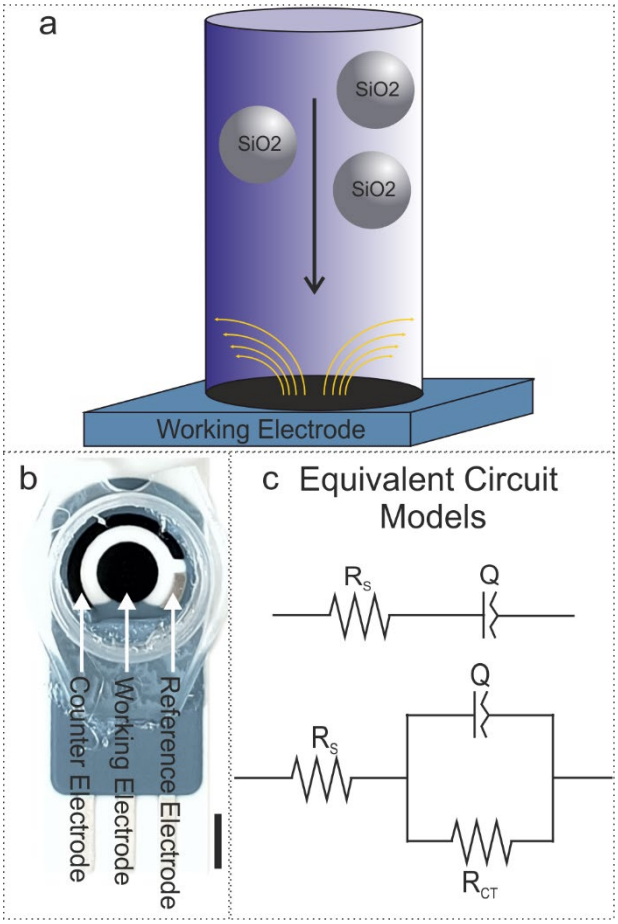

10.1002/anse.202400037

Figure 2. Potentiodynamic non-Faradaic EIS in blank electrolyte. (a) Cyclic voltammogram (CV) at 50 mV/s at a carbon SPE in 0.1 M KCl as blank electrolyte. (b) Bode plot of the impedance spectrum showing the measured impedance (points) in 0.1 M KCl at an applied potential of 0 V vs. Ag/AgCl. The lines show fits using two different models: R_s-Q and R_s - (Q || R_{CT}) models (refer to figure 1(c)). (c) The non-ideal capacitance (C_α) extracted using both the models as a function of the applied potential. (d) relative fit error in the parameter C_α using the two models. See figure S2 for other parameters. The lines in (b) and (c) are guides to the eye.

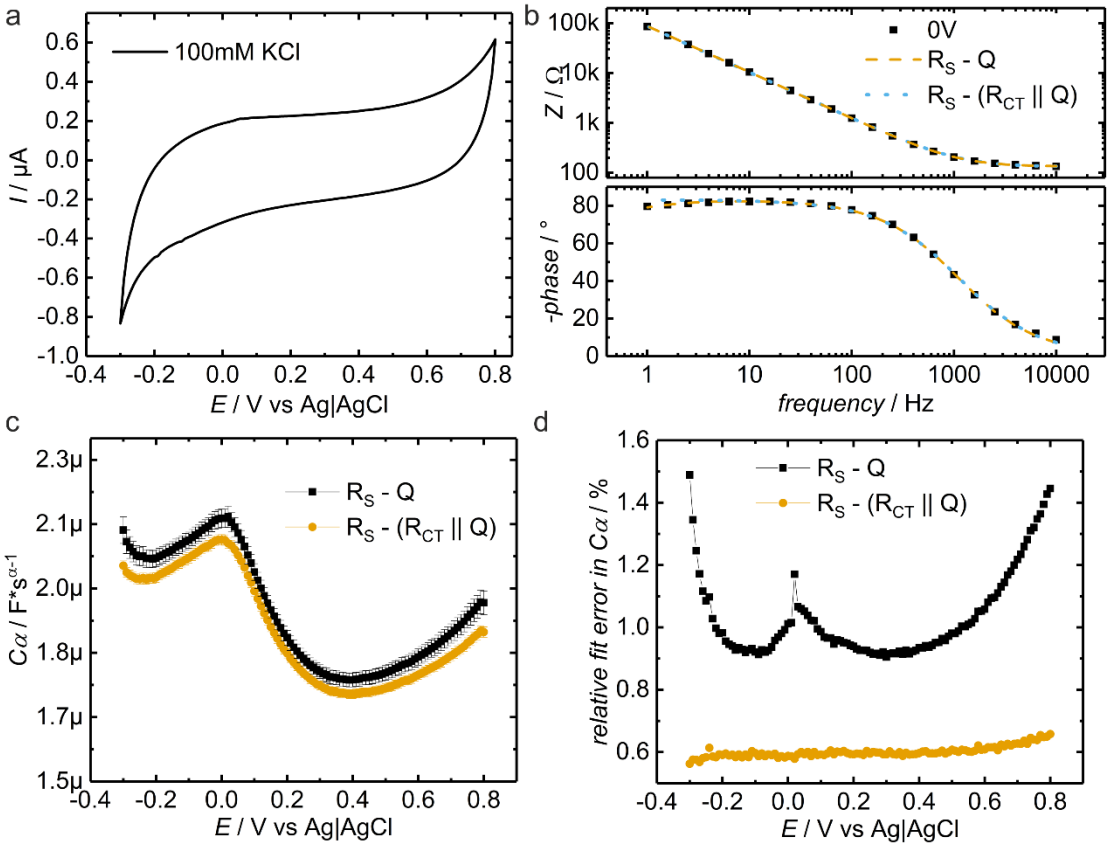

10.1002/anse.202400037

Figure 3. Time-differential potentiodynamic non-Faradaic EIS sensing of bead adsorption on carbon SPE. (a) Comparison of potential dependent C_α profile without (black squares) and with adsorbed silica beads (orange circles). (b) Time differential C_α profiles obtained by subtracting the curves in (a) from the curve measured in blank electrolyte. (c) Map of extracted C_α and (d) its time differential ΔC_α as a function of applied potential and time. The value of C_α is extracted using the R_s-Q model from impedance spectra measured at every potential, which is continuously repeated over time. The measurement starts in 0.1 M KCl for $\Delta t < 0$ min. The beads are added at $\Delta t = 0$ min. The time-differential map is calculated by subtracting the map in (a) from the potential-dependent C_α profile at $\Delta t = 0$ min. The value of α varies in the range of 0.85 – 0.90. The lines in (a) and (b) are guides to the eye.

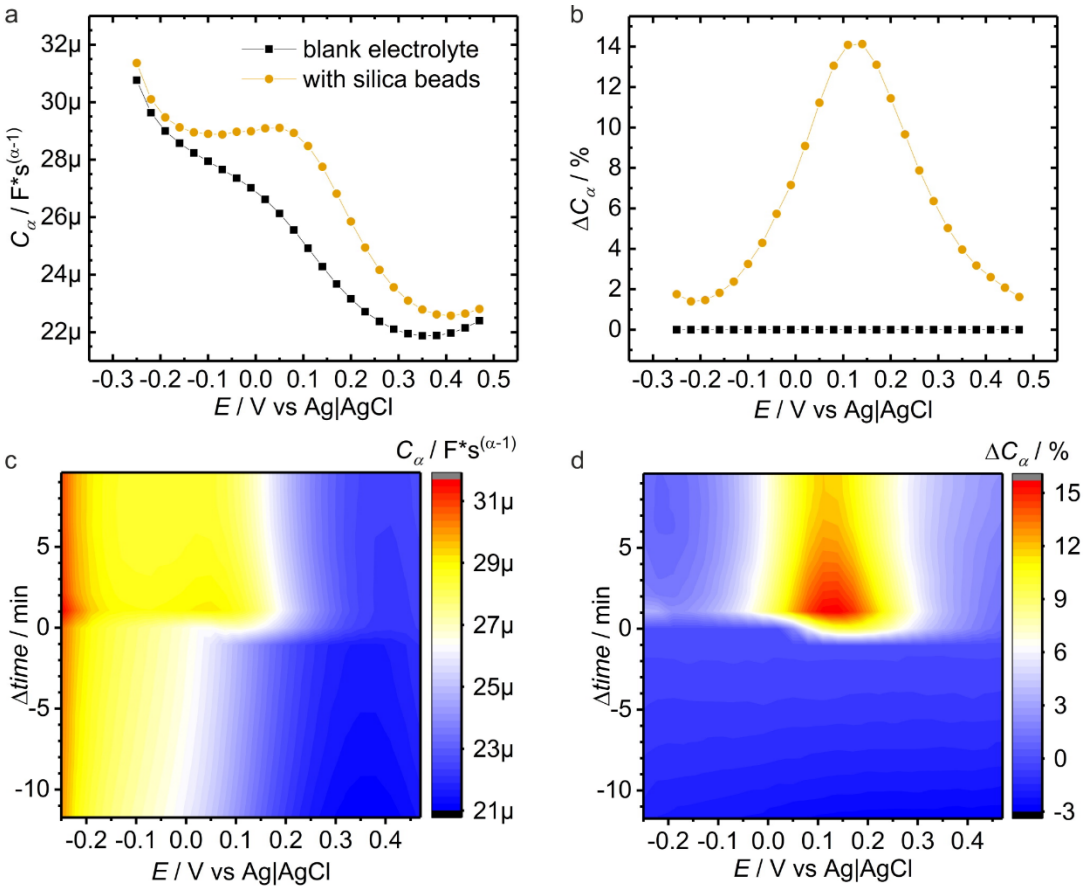

10.1002/anse.202400037

Figure 4. a) Map of the time differential of extracted R_s. The value of R_s is extracted from the same impedance dataset as used for figure 3 using the R_s-Q model. The differential is calculated similar to C_α in figure 3. The measurement starts in 0.1 M KCl for $\Delta t < 0$ min. The beads are added at $\Delta t = 0$ min. (b) Sensitivity of R_s to bead adsorption as a function of applied potential, calculated as the corresponding relative change in resistance obtained at $\Delta t = 2$ min. after the addition of beads. The line in (b) is a guide to the eye.

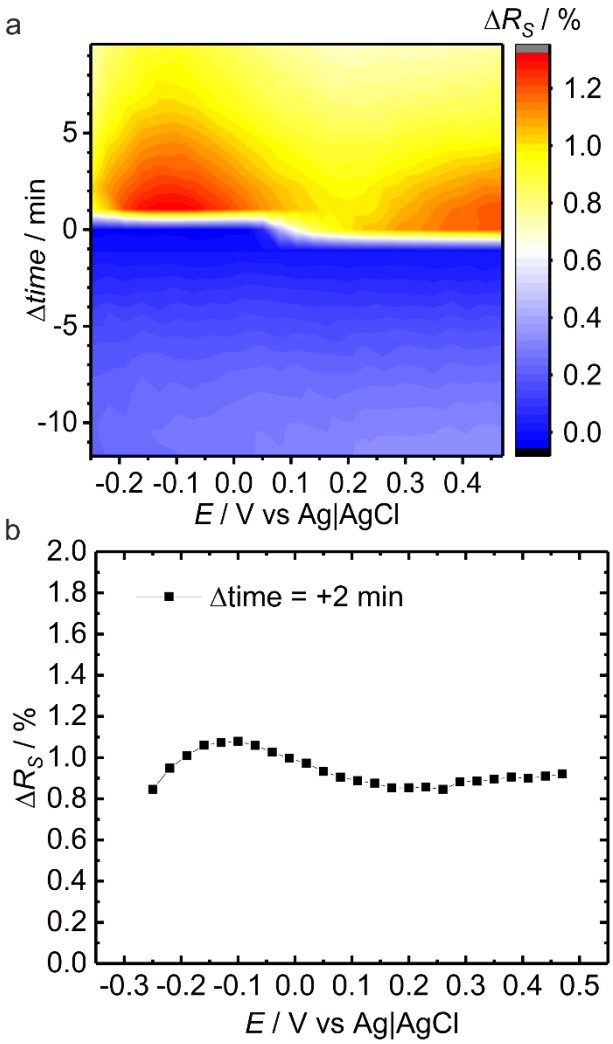

Figure 5. Time-differential potentiodynamic EIS sensing of bead adsorption, applied to the *Faradaic* case. Here, the EIS sensing trial is carried out in 0.1 mM ferrocenedimethanol (FDM) in 0.1 M KCl. (a) Map of the time-differential of extracted R_{CT} as a function of applied potential and time. The value of R_{CT} is extracted using the R_s - (Q || R_{CT}) model from impedance spectra measured at every potential, which is continuously repeated over time. The measurement starts in 0.1 M KCl with 0.1 mM FDM for $\Delta t < 0$ min. The beads are added at $\Delta t = 0$ min. The time-differential map is calculated by subtracting the R_{CT} profile from potential-dependent R_{CT} profile at $\Delta t = 0$ min. (b) Sensitivity (black points) as a function of applied potential, calculated as the corresponding relative change in charge transfer resistance obtained at $\Delta t = 2$ min. after the addition of beads. The CV of FDM is overlaid in orange. The line in (b) is a guide to the eye.

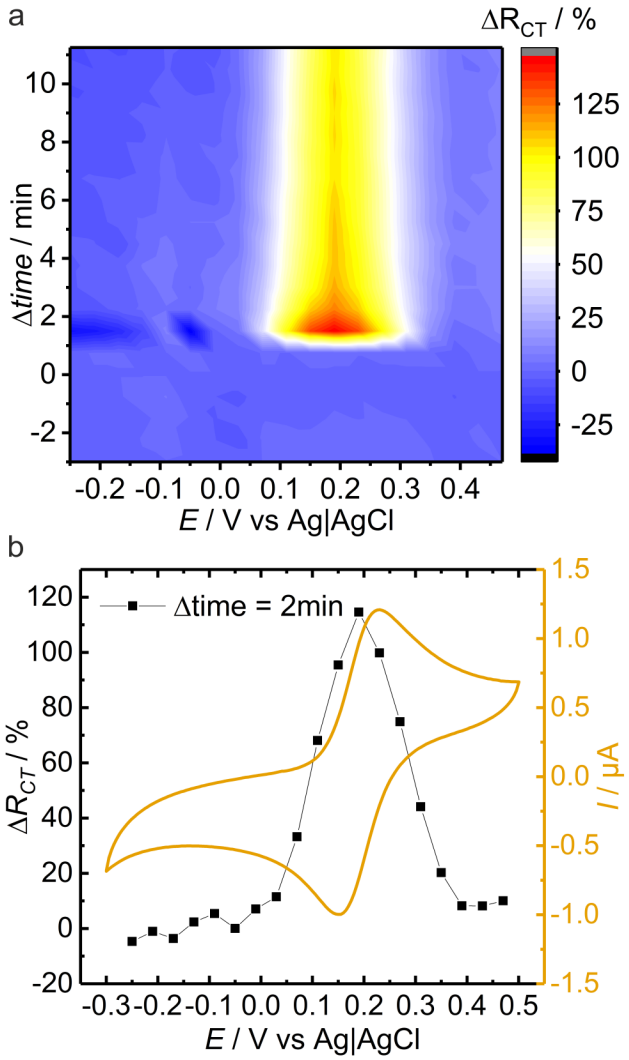

10.1002/anse.202400037

Figure 6. Time-differential potentiodynamic EIS sensing of cancer cell attachment (a,b) Maps of the time differential of C_α and R_s, which are extracted using the R_s-Q model from impedance spectra measured at every potential, continuously repeated over time. The measurement starts in 0.1 M KCl for $\Delta t < 0$ min. MCF-7 cancer cells are added at $\Delta t = 0$ min. (c) Comparison of potential dependent C_α profile without (black squares) and with adsorbed MCF-7 cells (brown spheres). The orange data points correspond to the profile at $\Delta t = 10$ min. (d) Time differential C_α profiles obtained by subtracting the response due to adsorbed cells from the curve measured in blank electrolyte. The value of α varies in the range of 0.93- 0.95. The lines in (c) and (d) are guides to the eye.

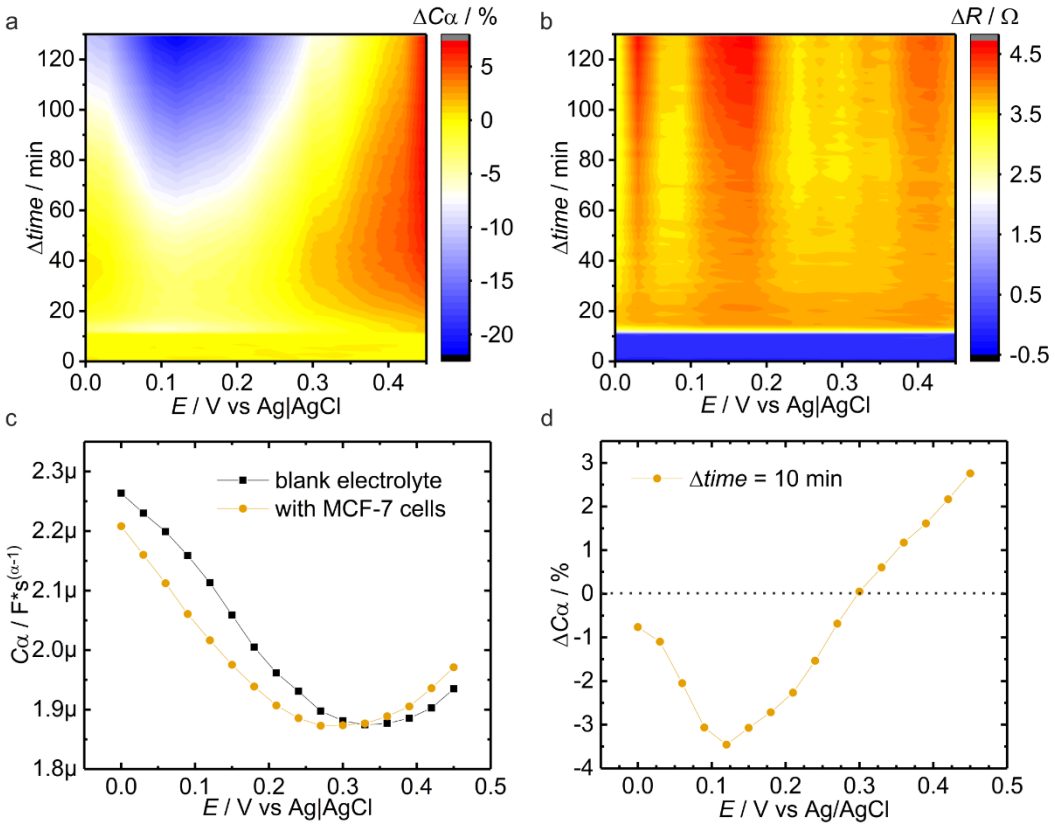

10.1002/anse.202400037

Table of Contents Figure

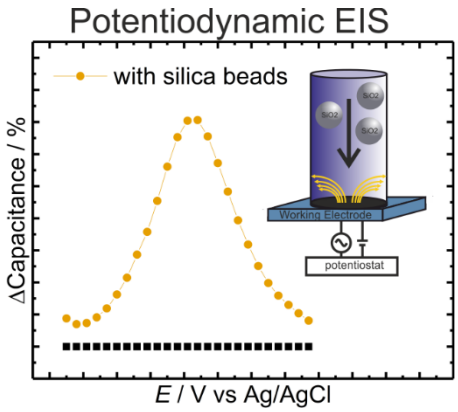

Table of Contents Running Text

We present a sensing strategy based on non-Faradaic electrochemical impedance spectroscopy augmented with potential cycling. We demonstrate that the sensitivity of capacitance due to bead sedimentation on to screen-printed carbon electrodes is dependent on the applied electrochemical potential. We exploit this strategy to sensitively detect cell attachment as a proof-of-principle demonstration.